ChemComm

Accepted Manuscript

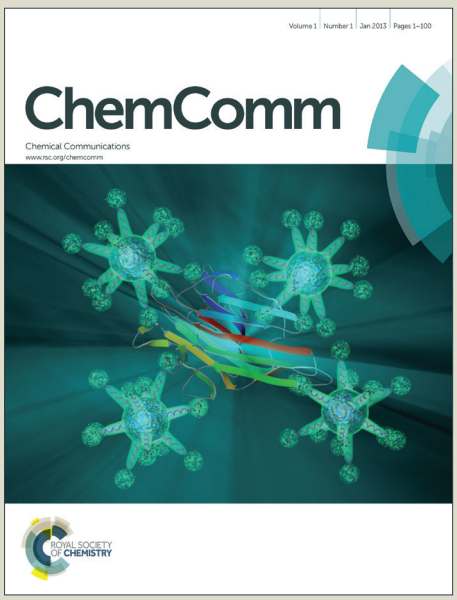

ROYAL SOCIETY OF CHEMISTRY

www.rsc.org/chemcomm

Journal Name

RSCPublishing

COMMUNICATION

Bicontinuous mesoporous carbon thin film via an order-order transition

Cite this: DOI: 10.1039/xoxxooooox

Guodong Deng,[a] Yuanzhong Zhang,[a] Changhuai Ye,[a] Zhe Qiang,[a] Gila E. Stein,[b] Kevin A. Cavicchi,[a] Bryan D. Vogt[a,*]

Received ooth March 2014,

DOI: 10.1039/xoxxooooox

www.rsc.org/chemcomm

Bicontinuous mesoporous carbon films are fabricated by cooperative self-assembly of phenolic resin and amphiphilic triblock copolymer via order-order transition from cylinders to gyroid. The film morphology is strongly influenced by the details of processing, including age of the resol, resol:template ratio, and the solvent vapor annealing process.

Chemical and physical properties of ordered mesoporous carbons (OMCs) are attractive for numerous applications, including separations, catalysis, energy conversion and energy storage.[1] Syntheses of OMCs through soft templating by organic-organic self-assembly[2] enable different mesostructures to be fabricated, including hexagonal (*p6mm*), body centered cubic ($Im\bar{3}m$), and 3-D bicontinuous ($Ia\bar{3}d$) mesostructures.[3] For many applications, the bicontinuous (gyroid) morphology is appealing due to its three-dimensional interconnected pore geometry.[4] Several templates have been reported for the synthesis of mesoporous carbon powders with gyroid mesostructure[3, 5] However in some cases, mesoporous carbon films are desirable due to their structural homogeneity and integrity.[1c] But unlike other mesostructures (*p6mm* and $Im\bar{3}m$),[6] the gyroid has not been demonstrated in thin films.

There are additional interface-based constraints that further narrow the phase window for bicontinuous morphologies. The processing window for bicontinuous morphologies can be significantly enlarged using ABC block copolymers (BCPs) as demonstrated by Wiesner and coworkers for mesoporous carbon powders.[5a] However when a triblock copolymer was applied to fabricate thin films, kinetically trapped morphologies were formed due to competition between ordering and crosslinking kinetics.[7] For neat block copolymer (BCP) thin films, solvent vapor annealing (SVA) can generally be used to effectively enhance their ordering and SVA has been applied to gyroidal thin films.[18, 19] For fabrication of mesoporous carbon films, SVA has been primarily used with cylinder-forming AB BCP/carbon precursor mixtures.[8,9]

Here, we seek to fabricate highly ordered bicontinuous mesoporous carbon films using both cooperative assembly and SVA process techniques. In this work, poly (ethylene oxide)-*block*-poly(ethyl acrylate)-*block*-polystyrene, OES (PEO_{45}-b-PEA_{117}-b-PS_{99}), a non-frustrated[10] amphiphilic triblock block copolymer (f_{PEO} = 8%, f_{PEA} = 47%, f_{PS} = 45%; M_n = 24 kDa; Đ =1.2),[7] is used to cooperatively assemble with phenolic resin oligomers (resol), which is the carbonizable precursor. The morphology of the OES/resol mixtures is impacted by the relative resol content similar to homopolymer[11] loading in other ABC BCPs. Films were prepared by spin coating, followed by SVA using nearly saturated MEK vapor. MEK is a good solvent for each segment of the triblock copolymer and resol with a slight selectivity for the PEA segments.[7] As shown in the Electronic Supplementary Information (ESI) Fig. S1, the solvent reservoir for SVA is almost completely empty after 2 h as determined by *in-situ* ellipsometry measurements of the film thickness during SVA.

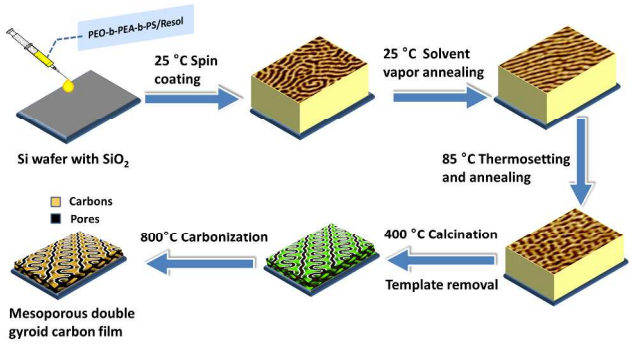

Scheme 1. Schematic representation of the fabrication of mesoporous carbons via cooperative self-assembly induced by a solvent vapor annealing process followed by thermally induced self-assembly, calcination and carbonization.

Two different SVA protocols have been utilized: single SVA with fast drying and double SVA with slow drying. For a single SVA process, the film is exposed to saturated MEK vapor for 1 h, followed by re-filling the solvent chamber and solvent annealing for another 2 h with a fast drying by removing films and directly exposing to the ambient environment. For the double SVA process, the film is exposed to the saturated MEK vapor for over 3 h first until dry, followed by re-filling the solvent reservoir and then continuing the same SVA process for > 3 h to ensure that the film is slowly dried.

Post SVA procedures followed standard mesoporous carbon fabrication: thermopolymerization, calcination and carbonization as illustrated in Scheme 1. Fabrication details are included in the ESI.

Atomic force microscopy (AFM) was employed to characterize the surface morphologies for each processing step. For as-spun films prior to SVA, poorly ordered short cylindrical rods are observed on the surface of films (Fig. S2). These disorganized, but self-assembled structures result from the rapid drying during spin coating. Exposure to MEK vapor significantly increases the polymer mobility to yield well-organized mesostructures. As expected, the morphology strongly depends on composition, i.e., resol content (Fig. 1). For the pure triblock copolymer, spheres of PEO (minority component) are found (Fig. 1A). The addition of resol to the OES triblock copolymer acts to swell the PEO phase, effectively increasing its volume fraction and enabling different morphologies to be traversed. The trajectory across the phase diagram maps is effectively modifying the volume fraction.[12] The ternary phase diagram can lead to non-obvious trajectories with a wide array of morphologies with the addition of selective polymers.[12] However, there is a subtle difference as the interaction parameters are also impacted due to the difference between resol and PEO for the interactions with PEA and PS.

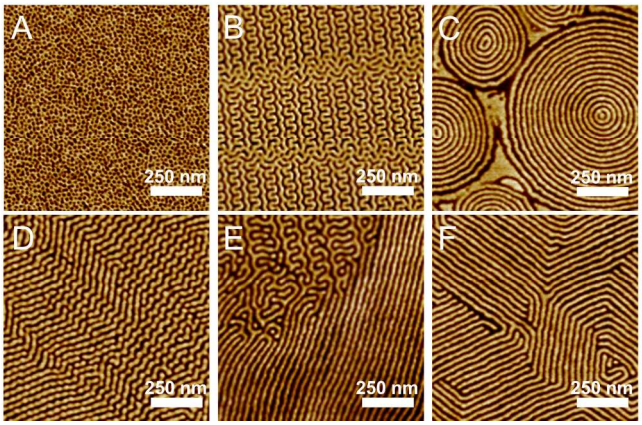

Fig. 1 AFM phase images of films containing (A) 0 wt.%; (B) 25 wt.%; (C) 40 wt.%; (D) 50 wt.%; (E) 60 wt.% and (F) 67 wt.% resol after exposure to MEK using single SVA process. The resol used to fabricate these films was ~17 weeks old.

At 25 wt.% resol, the distinctive "double wave" pattern consistent with the gyroid morphology is observed (Fig. 1B) after the single SVA process. At 40 wt.% resol, almost onion-like, concentric rings (Fig. 1C) are observed, which is reminiscent of multi-layered vesicles;[13] the high degree of curvature near the center of the target patterns is not favorable for cylinders, so we attribute this structure to lamellae. At this composition, the film is nearly 50 % hydrophilic and 50 % hydrophobic, so the formation of lamellae is not fully unexpected. Increasing the resol concentration further to 50 wt.%, the wavy line structure is consistent with the gyroid morphology (Fig. 1D); there are multiple short straight line defects that could be consistent either lamellae or cylinders. At 60 wt.% resol, a gyroid structure that co-exists with long straight lines is observed (Fig. 1E). Based on the progression, these data suggest that the straight defects in Fig. 1D are likely perpendicular lamellae. Similarly as further increasing the resol concentration to 67 wt.% results in the formation of parallel cylinders with sharp bends (Fig. 1F), the gyroid morphology in Fig. 1E is likely in co-existence with cylinders. Nonetheless, MEK enables reorganization into well-ordered morphologies.

In comparing the two extreme compositions that produce gyroid mesostructures, the interdomain spacing of $(100)_G$ (i.e., $d_{(100)G}$ or lattice parameter α_G) from AFM phase images increases from 53 ± 1 nm to 63 ± 1 nm for 25 wt.% and 60 wt.% resol, respectively. This ~10 nm increase in d-spacing is consistent with domain swelling by the resol. However, when these two gyroid films were heated (85 °C) to thermopolymerize the resol, the gyroid morphology transforms to either dot (25 wt.% resol) or line (60 wt.% resol) pattern as shown in Fig. S3. Thermopolymerization at higher temperatures also results in this transformation. As crosslinking of the resol decreases the hydroxyl concentration, the effective Flory-Huggins interaction parameter, χ_{eff}, is expected to decrease based prior work involving hydrogen bonding of additives with PEO.[14] However, the molecular weight increases during thermopolymerization and the specific volume of the resol decreases to shift the relative fraction of the block copolymer to alter the effective volume fractions. These changes in the volume fraction and interaction parameter on heating may be responsible for the change in structure due to an order-order transition (OOT), but kinetically trapped morphologies are possible during SVA due to slight selectivity of MEK for the PEA segments.[15]

As the 25 wt.% resol film exhibits the gyroid without co-existence of an additional phase and the low carbonizable content for high porosity, this composition is examined more carefully to test if the OOT change in morphology is kinetic or thermodynamic in nature. For the single SVA that was utilized, the SVA may be insufficient as both time of exposure and rate of drying impact ordering.[16] The double SVA procedure provides additional time for the morphology to evolve to promote the formation of an equilibrium nanostructure. With this double SVA processing, the surface morphology appears to be parallel cylinders (Fig. 2A), which suggests the gyroid was kinetically trapped by the single SVA process. The morphology evolution from gyroid to parallel cylinders with increasing solvent annealing time has been reported for neat BCPs.[9]

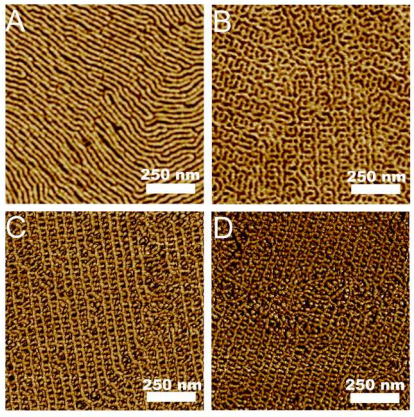

Fig. 2 AFM phase images of film containing 25 wt.% resol (A) after double SVA; (B) 85 °C, thermopolymerized; (C) 400 °C, calcined; (D) 800 °C, carbonized. The resol in these studies was ~ 8 weeks old.

Interestingly, unlike the transition from gyroid to a dot pattern on thermopolymerization at 85 °C previously shown for the single SVA procedure, an OOT from parallel cylinder to gyroid oriented along the (211) direction occurs with the double

SVA (Fig. 2B). The $d_{(100)G}$ (lattice parameter) of thermopolymerized film is nearly identical to that obtained after single SVA (Fig. 1B). This behavior suggests the structure obtained on thermopolymerization is dependent on the prior mesostructure and implies a delicate balance between thermodynamics and kinetics. There are multiple ordered grains present in the AFM micrograph (Fig. 2B); these smaller grains are similar to those observed after double SVA despite the change in space group. This consistency is suggestive of the epitaxial relationship between the initial cylinders and the final gyroid morphology on thermopolymerization as observed for neat BCPs.[17]

This gyroid mesostructure can be maintained after the BCP template is removed at 400 °C in N_2 (Fig. 2C). This morphology is similar to that observed for mesoporous polymer thin films that were formed by the chemical degradation of one block and its subsequent removal.[18] As expected, the gyroid mesostructure demonstrates high porosity (~ 50%) as determined by ellipsometric porosimetry (Fig. S4). Additionally, the mesoporous gyroid morphology has a narrow pore size distribution with pore size of 12 ± 2 nm (Fig. 2C). Moreover, the film thickness is significantly reduced from 515 nm to 124 nm (76 % contraction) during the calcination process due to stress developed during the template removal. However, this contraction is similar to other mesoporous carbon films that contract by 68 %.[19] For the gyroid film examined here, some defects form on the surface on calcination that do not appear in the thermopolymerized sample. We speculate that these defects are caused by stresses associated with the calcination process that leads to further crosslinking of the resol along with template removal. This gyroid morphology with defects is consistently observed across the film. Upon carbonization at 800 °C, the surface morphology is almost invariant from that of the calcined film (Fig. 2D), which illustrates the thermal stability of the gyroid. Thus, the critical step to obtaining the gyroid morphology appears to be the crosslinking where the structure is chemically locked in place.

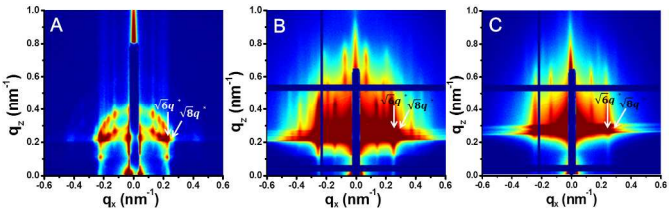

Fig. 3 The GISAXS pattern of film containing 25 wt.% resol after double SVA at incident angelαi = 0.10°, (A) 85 °C, thermopolymerized; (B) 400 °C, calcined; (C) 800 °C, carbonized. The resol in these studies was ~ 8 weeks old.

To further examine the gyroid morphology in thermo-polymerized film (Fig. 2B), grazing incidence small angle X-ray scattering (GISAXS) is used to elucidate the mesostructure. Fig. 3A illustrates the GISAXS pattern from OES/resol thermopolymerized film before template removal. The GISAXS pattern shows discrete diffraction spots with some peak broadening in semi-circular arrangement that are consistent with the gyroid structure possessing $Ia\bar{3}d$ symmetry with preferential alignment of the (211) plane parallel to the substrate,[20a, 20b] which agrees with the AFM observations (Fig. 2B). The ratio of the second and first diffraction spots is determined to be 1.16 in agreement with the predicted value of $\sqrt{8}/\sqrt{6}$ for the (220) and (211) reflections of the gyroid structure. From the primary peak position at $\sqrt{6}q^* = 0.245$ nm^{-1}, the d_{100} spacing (lattice parameter) estimated from GISAXS is 62.6 nm ($d_{100}=2\pi/q^*$), which is larger than that determined by AFM (53 ± 1 nm). After template removal, two primary diffraction peaks remain with the ratio of $\sqrt{8}/\sqrt{6}$, which is consistent with the gyroid structure (Fig. 3B). However, some generally "forbidden" reflections are present in the GISAXS pattern due to uniaxial compression perpendicular to the substrate. Similar distortion of the gyroid structure ($Ia\bar{3}d$ symmetry) has been reported after template removal for inorganic structures.[20a, 21] After carbonization, the distortion of gyroid structure is more severe due to the large uniaxial contraction of the film (Fig. 3C). Despite this, the gyroid mesostructure can still be verified by GISAXS (Fig. 3C) due to the reflections at q* ratios of $\sqrt{6}$ and $\sqrt{8}$.

In addition to the processing sensitivity, the compositional window for the gyroid morphology after resol crosslinking transformed from parallel cylinders after SVA using identical SVA processing can be significantly altered by the aging of the resol. Even with storage of the nominally neutral (pH = 7), ethanoic resol solution in a refrigerator ($\approx$ 5 °C), the compositional window for the parallel cylinders after the double SVA procedure is shifted by several percent as 25.0 wt.% resol leads to what is attributed to perpendicular cylinders (if the resol is aged 6 mo.) as supported by AFM (Fig S5A) and GISAXS (Fig. S6), but the parallel cylinders can be partially recovered by increasing the resol content to 33.3 wt.% after double SVA (Fig. S5C). Similarly, this morphology is fully transformed to the same gyroid structure after heating (Fig. S5I). Another interesting observation is that the gyroid structure can be obtained by double SVA as shown in AFM (Fig. S5B) and GISAXS (Fig. S7 & S8). This strong dependence on multiple processing parameters is reminiscent of the challenges identified by Hillhouse and co-workers for the fabrication of mesoporous silica films with the gyroid morphology.[22] In particular, the age of the silica sol prior to casting the film can impact the morphology observed due to changes in the interfacial curvature induced by extent of condensation.[22] For mesoporous silica films, a transformation from 2D hexagonal to gyroid to lamellae was observed as the silica sol aging time was increased. However in the case of the resol-BCP system, changes in the equilibrium phase can occur as the resol crosslinks, so balance between the structure formed by SVA, equilibrium structure and the mobility of the system during crosslinking determines the details of the final morphology. This sensitivity to the resol aging and the potential OOT during crosslinking likely explains why the gyroid has not been reported in thin films for soft templated mesoporous carbons.

Conclusions

Long-range ordered gyroidal (cubic; $Ia\bar{3}d$) mesoporous carbon film can be fabricated using OES/resol cooperative assembly processed by double solvent vapor annealing and post thermal annealing process that induces an order-order transition from parallel cylinder to the gyroid. Direct single solvent vapor annealing of the same composition to gyroid leads to non-gyroid morphologies on thermopolymerization. After stabilization by thermopolymerization, the gyroid mesostructure is maintained through calcination and carbonization.

This work was partially supported by the National Science Foundation under grant number CBET-1159295. Research was carried out in part at the Center for Functional Nanomaterials,

Brookhaven National Laboratory, which is supported by the U.S. Department of Energy, Office of Basic Energy Sciences, under Contract DE-AC02-98CH10886. Use of the Advanced Photon Source, an Office of Science User Facility operated for the U.S. Department of Energy (DOE) Office of Science by Argonne National Laboratory, was supported by the U.S. DOE under Contract No. DE-AC02-06CH11357.

Notes and references

[a] Department of Polymer Engineering, The University of Akon, Akron OH 44325
[b] Department of Chemical and Biomolecular Engineering, University of Houston, Houston, TX 77204
* E-mail: vogt@uakron.edu; Tel: (+01) 330-972-8608

1. (a) Y. Ye, C. Jo, I. Jeong and J. Lee, *Nanoscale*, 2013, **5**, 4584-4605; (b) Z. X. Wu and D. Y. Zhao, *Chem. Commun*., 2011, **47**, 3332-3338; (c) D. Feng, Y. Y. Lv, Z. X. Wu, Y. Q. Dou, L. Han, Z. K. Sun, Y. Y. Xia, G. F. Zheng and D. Y. Zhao, *J. Am. Chem. Soc.*, 2011, **133**, 15148-15156; (d) A. Taguchi and F. Schuth, *Micropor. Mesopor. Mat.*, 2005, **77**, 1-45; (e) R. Ryoo, S. H. Joo, M. Kruk and M. Jaroniec, *Adv. Mater.*, 2001, **13**, 677-681.
2. (a) C. D. Liang, K. L. Hong, G. A. Guiochon, J. W. Mays and S. Dai, *Angew. Chem. Int. Ed.*, 2004, **43**, 5785-5789; (b) Y. Meng, D. Gu, F. Q. Zhang, Y. F. Shi, H. F. Yang, Z. Li, C. Z. Yu, B. Tu and D. Y. Zhao, *Angew. Chem. Int. Ed.*, 2005, **44**, 7053-7059.
3. Y. Meng, D. Gu, F. Q. Zhang, Y. F. Shi, L. Cheng, D. Feng, Z. X. Wu, Z. X. Chen, Y. Wan, A. Stein and D. Y. Zhao, *Chem. Mater.*, 2006, **18**, 4447-4464.
4. D. A. Hajduk, P. E. Harper, S. M. Gruner, C. C. Honeker, G. Kim, E. L. Thomas and L. J. Fetters, *Macromolecules*, 1994, **27**, 4063-4075.
5. (a) J. G. Werner, T. N. Hoheisel and U. Wiesner, *ACS Nano*, 2014, **8**, 731-743; (b) J. G. Li, Y. D. Lin and S. W. Kuo, *Macromolecules*, 2011, **44**, 9295-9309.
6. (a) J. Schuster, R. Koehn, A. Keilbach, M. Doeblinger, H. Amenitsch and T. Bein, *Chem. Mater.*, 2009, **21**, 5754-5762; (b) L. Song, D. Feng, C. G. Campbell, D. Gu, A. M. Forster, K. G. Yager, N. Fredin, H.-J. Lee, R. L. Jones, D. Zhao and B. D. Vogt, *J. Mater. Chem.*, 2010, **20**, 1691-1701.
7. G. Deng, Z. Qiang, W. Lecorchick, K. A. Cavicchi and B. D. Vogt, *Langmuir*, 2014, **30**, 2530-2540.
8. Z. Qiang, J. C. Xue, K. A. Cavicchi and B. D. Vogt, *Langmuir*, 2013, **29**, 3428-3438.
9. (a) C. X. Luo, W. H. Huang and Y. C. Han, *Macromol. Rapid Comm.*, 2009, **30**, 515-520; (b) M. S. She, T. Y. Lo and R. M. Ho, *Macromolecules*, 2014, **47**, 175-182.
10. J. Qin, F. S. Bates and D. C. Morse, *Macromolecules*, 2010, **43**, 5128-5136.
11. M. S. Tureau, W.-F. Kuan, L. Rong, B. S. Hsiao and T. H. Epps, III, *Macromolecules*, 2012, **45**, 4599-4605.
12. M. S. Tureau, L. Rong, B. S. Hsiao and T. H. Epps, III, *Macromolecules*, 2010, **43**.
13. P. Zou and C. Y. Pan, *Macromol. Rapid Comm.*, 2008, **29**, 763-771.
14. V. K. Daga and J. J. Watkins, *Macromolecules*, 2010, **43**, 9990-9997.
15. C. Sinturel, M. Vayer, M. Morris and M. A. Hillmyer, *Macromolecules*, 2013, **46**, 5399-5415.
16. J. N. L. Albert, W.-S. Young, R. L. Lewis, III, T. D. Bogart, J. R. Smith and T. H. Epps, III, *ACS Nano*, 2012, **6**, 459-466.
17. C. Wang, K. Jiang, P. W. Zhang and A. C. Shi, *Soft Matter*, 2011, **7**, 10552-10555.
18. E. J. W. Crossland, S. Ludwigs, M. A. Hillmyer and U. Steiner, *Soft Matter*, 2010, **6**, 670-676.
19. S. Tanaka, Y. Katayama, M. P. Tate, H. W. Hillhouse and Y. Miyake, *J.Mater. Chem.*, 2007, **17**, 3639-3645.
20. (a) E. J. W. Crossland, M. Kamperman, M. Nedelcu, C. Ducati, U. Wiesner, D. M. Smilgies, G. E. S. Toombes, M. A. Hillmyer, S. Ludwigs, U. Steiner and H. J. Snaith, *Nano Lett*, 2009, **9**, 2807-2812; (b) B. Lee, I. Park, J. Yoon, S. Park, J. Kim, K. W. Kim, T. Chang and M. Ree, *Macromolecules*, 2005, **38**, 4311-4323.
21. (a) H. Y. Hsueh, H. Y. Chen, M. S. She, C. K. Chen, R. M. Ho, S. Gwo, H. Hasegawa and E. L. Thomas, *Nano Lett*, 2010, **10**, 4994-5000; (b) H. Y. Hsueh, Y. C. Huang, R. M. Ho, C. H. Lai, T. Makida and H. Hasegawa, *Adv. Mater.*, 2011, **23**, 3041-3046.
22. V. N. Urade, L. Bollmann, J. D. Kowalski, M. P. Tate and H. W. Hillhouse, *Langmuir*, 2007, **23**, 4268-4278.

